UDC 539.3
DOI: https://doi.org/10.26642/tn-2019-1(83)-59-68

N. Ilchuk, PhD, Associated Professor
Ia. Pasternak, PhD, DSc, Professor
Lutsk National Technical University

Boundary element method for fracture mechanics analysis of 3d non-planar cracks in anisotropic solids

Among the numerical approaches to fracture mechanics analysis of cracked anisotropic solids, the boundary element method is notable for high accuracy and performance due to its semi-analytical nature and the use of only boundary mesh. Various boundary element techniques were proposed for 3D fracture mechanics analysis. However, the main problem of these approaches is the treatment of singular and hypersingular integrals, which can demand analytic evaluation of coefficient at kernel singularity at singular point in local curvilinear coordinates, which produce cumbersome equations in the case of non-planar geometries.

Therefore, the paper presents novel formulation of the boundary element method for 3D fracture mechanics analysis of anisotropic solids with non-planar cracks. Pan's single domain boundary element formulation is extended with several novelties, which allow accurate analysis of non-planar geometries. These are modified Kutt's numerical quadratures with Chebyshev nodes for accurate evaluation of singular and hypersingular integrals; polynomial mappings for smoothing the integrand at the crack front line; and special shape functions, which account for a square-root stress singularity at crack front and allow accurate determination of stress intensity factors. The kernels of boundary integral equations are evaluated using the exponentially convergent quadrature, which allows derivation of fast boundary element technique. The procedure for accurate numerical determination of stress intensity factors at arbitrary point of the crack front is also developed. Numerical examples are presented, which show high accuracy of the proposed boundary element method. It is shown that non-planar cracks exhibit shearing mode opening along with normal one due to its geometry and direction of the applied loading.

Present approach can be combined with Sih's strain energy density criterion to study 3D cracks propagation in anisotropic elastic solids under fatigue loading, which is the direction of future research.

Keywords: *anisotropic; crack; boundary element method; 3D fracture; hypersingular.*

1. Introduction

Composite anisotropic materials are widely used in modern technology. They are lighter and possess high strength and durability. Composite materials can be designed to fit the demands on bearing capacity of particular structural element, in contrast to traditional ones, which are mainly isotropic, and act in the same way in different directions.

Such broad usage of composite materials raised issues on their fracture. There have been introduced two main models of such materials. The first of them considers internal structure of a composite, and studies fracture phenomena caused by fiber delamination, fiber rupture etc. The second one assumes that a composite material is an anisotropic homogeneous continuum, and models fracture phenomena caused by cracks, notches, wedges etc. Sih [1, p. 20] has shown that homogeneous anisotropic model can be successfully applied to fracture analysis of composite materials, and stress intensity factors (which are incorporated in Sih's strain energy density criterion) are determinative in estimation of composite fracture.

Among the numerical approaches for fracture mechanics analysis of cracked anisotropic solids, the boundary element method (BEM) is notable for high accuracy and performance due to its semi-analytical nature and the use of only boundary mesh. Various boundary element techniques were proposed for 3D fracture mechanics analysis. Mi and Aliabadi [2, p. 161] derived a 3D dual BEM for analysis of 3D cracks in isotropic linear elastic solids. However, this approach used semi-analytic singularity subtraction technique for integration of hypersingular integrals. There are different modifications of this technique however, it has to be seriously modified, when applied to analysis of anisotropic solids.

Saez et al. [5, p. 287] presented a boundary element formulation for crack analysis in transversely isotropic solids. Muñoz-Reja et al. [6, p. 15] presented the 3D BEM for fracture mechanics analysis of anisotropic magnetoelectroelastic materials. However, these approaches used subregion technique, which introduces additional boundaries and thus computational error to stress intensity factors obtained.

Jaworski et al. [7, p. 295], Nikolskiy et al. [8, p. 44] presented 3D BEM for fracture mechanics analysis of non-planar cracks; however, planar triangular elements are used, which introduce error in modeling of crack geometry. The same planar elements are used in Galerkin BEM for evaluation of singular terms.

In contrast to above mentioned papers, Pan and Yuan developed a single-domain BEM for 3D fracture mechanics analysis in generally anisotropic solids. Quadratic quadrilateral elements were used, which precisely

© N. Ilchuk, Ia. Pasternak, 2019

model smooth non-planar cracks. However, the main problem of this approach is the quadrature used for treatment of singular and hypersingular integrals, which demand analytic evaluation of coefficient at kernel singularity at singular point in local curvilinear coordinates, which produce cumbersome equations in the case of non-planar geometries. Therefore, Pan and Yuan restrict themselves in this paper to the flat crack surfaces only.

This paper presents a novel single-domain BEM for analysis of 3D non-planar cracks in anisotropic solids, which consists of new quadratures for hypersingular integrals, new approaches for accurate evaluation of stress intensity factors, and accurate techniques for fast and accurate evaluation of hypersingular kernels.

2. Boundary integral equations for cracked anisotropic solids

In a fixed Cartesian coordinate system $Ox_1x_2x_3$ the equilibrium equations of an anisotropic solid can be presented in the following compact form

$$\sigma_{ij,j} + f_i = 0, \tag{1}$$

where σ_{ij} is a stress tensor; f_i is a body force vector; and indices vary from 1 to 3 (i.e. $i = 1,2,3$). Here and further the Einstein summation convention is used. A comma at subscript denotes differentiation with respect to a coordinate indexed after the comma, i.e. $u_{i,j} = \partial u_i / \partial x_j$.

In the assumption of small strains the constitutive equations of linear anisotropic elasticity in the compact notations are as follows

$$\sigma_{ij} = C_{ijkm} u_{k,m}, \tag{2}$$

where u_i is a displacement vector; C_{ijkm} are the elastic stiffnesses (elastic moduli).

The boundary value problem for partial differential equations (1), (2) can be reduced to the solution of the following boundary integral equations of the single domain BEM:

- when the collocation point $\mathbf{x}_0$ is placed on the smooth part of the boundary $\partial\mathcal{B}$ of the solid $\mathcal{B}$:

$$\begin{aligned}\frac{1}{2}u_i(\mathbf{x}_0) = &\iint_{\partial\mathcal{B}} U_{ij}(\mathbf{x},\mathbf{x}_0) t_j(\mathbf{x}) dS(\mathbf{x}) - \mathrm{CPV}\iint_{\partial\mathcal{B}} T_{ij}(\mathbf{x},\mathbf{x}_0) u_j(\mathbf{x}) dS(\mathbf{x}) \\ &+ \iint_{C} U_{ij}(\mathbf{x},\mathbf{x}_0) \Sigma t_j(\mathbf{x}) dS(\mathbf{x}) - \mathrm{CPV}\iint_{C} T_{ij}(\mathbf{x},\mathbf{x}_0) \Delta u_j(\mathbf{x}) dS(\mathbf{x}), \\ &+ \iiint_{\mathcal{B}} U_{ij}(\mathbf{x},\mathbf{x}_0) f_j(\mathbf{x}) dV(\mathbf{x}),\end{aligned} \tag{3}$$

- when the collocation point $\mathbf{x}_0$ is placed on the smooth part of the crack surface C:

$$\begin{aligned}\frac{1}{2}\Delta t_i(\mathbf{x}_0) = n_j(\mathbf{x}_0)\Bigg[&\mathrm{CPV}\iint_{C} D_{ijk}(\mathbf{x},\mathbf{x}_0) \Sigma t_k(\mathbf{x}) dS(\mathbf{x}) \\ &- \mathrm{HFP}\iint_{C} S_{ijk}(\mathbf{x},\mathbf{x}_0) \Delta u_k(\mathbf{x}) dS(\mathbf{x}) + \iint_{\partial\mathcal{B}} D_{ijk}(\mathbf{x},\mathbf{x}_0) t_k(\mathbf{x}) dS(\mathbf{x}), \\ &- \iint_{\partial\mathcal{B}} S_{ijk}(\mathbf{x},\mathbf{x}_0) u_k(\mathbf{x}) dS(\mathbf{x}) + \iiint_{\mathcal{B}} D_{ijk}(\mathbf{x},\mathbf{x}_0) f_k(\mathbf{x}) dV(\mathbf{x})\Bigg],\end{aligned} \tag{4}$$

which kernels are defined as

$$U_{ij}(\mathbf{x},\mathbf{x}_0) = \frac{1}{8\pi^2 |\mathbf{x}-\mathbf{x}_0|} \oint_{|\boldsymbol{\lambda}|=1} \Gamma_{ij}^{-1}(\boldsymbol{\lambda}) dl(\boldsymbol{\lambda}), \quad T_{qi}(\mathbf{x},\mathbf{x}_0) = \tilde{C}_{ijkm} n_j(\mathbf{x}) U_{qk,m}(\mathbf{x},\mathbf{x}_0); \tag{5}$$

$$D_{ijk} = -\tilde{C}_{ijmp} U_{mk,p}, \quad S_{ijk} = -\tilde{C}_{ijmp} \tilde{C}_{kqrs} n_q U_{mr,ps}, \tag{6}$$

$$\begin{aligned}U_{ij,k}(\mathbf{x},\mathbf{x}_0) &= -\frac{1}{8\pi^2 r^2} \oint_{|\boldsymbol{\lambda}|=1} \left[\tau_k \Gamma_{ij}^{-1}(\boldsymbol{\lambda}) + \lambda_k F_{ij}\right] dl(\boldsymbol{\lambda}), \\ U_{ij,km}(\mathbf{x},\mathbf{x}_0) &= \frac{1}{8\pi^2 r^3} \oint_{|\boldsymbol{\lambda}|=1} \Big[2\Gamma_{ij}^{-1}(\boldsymbol{\lambda})\tau_k\tau_m + 2F_{ij}(\tau_k\lambda_m + \tau_m\lambda_k) \\ &\quad - \lambda_k\lambda_m \Big[2\Gamma_{ip}^{-1}(\boldsymbol{\lambda}) \tilde{C}_{plqs} \tau_l \tau_s \Gamma_{qj}^{-1}(\boldsymbol{\lambda}) \\ &\quad + \left(F_{ip}\Gamma_{qj}^{-1}(\boldsymbol{\lambda}) + \Gamma_{ip}^{-1}(\boldsymbol{\lambda}) F_{qj}\right) \tilde{C}_{plqs}(\tau_l\lambda_s + \tau_s\lambda_l)\Big]\Big] dl(\boldsymbol{\lambda});\end{aligned} \tag{7}$$

where n_p is a unit outwards normal vector to the surface $\partial\mathcal{B}$; $\Sigma f = f^+ + f^-$ and $\Delta f = f^+ - f^-$ denote the sum and the difference of functions on opposite faces C^+ and C^- of the crack surface C; $t_i = \sigma_{ij} n_j$ is the traction vector; $\boldsymbol{\tau}$ is a unit vector collinear with $\mathbf{x}-\mathbf{x}_0$; and $\boldsymbol{\lambda}$ is a unit vector normal to $\mathbf{x}-\mathbf{x}_0$; $r = |\mathbf{x}-\mathbf{x}_0|$; $\Gamma_{ij}^{-1}(\boldsymbol{\xi})$ are

the components of the matrix, which is inverse of the matrix $\Gamma_{ik}(\boldsymbol{\xi}) = \tilde{C}_{ijkm}\xi_j\xi_m$, i.e. $\Gamma^{-1}_{ik}(\boldsymbol{\xi})\Gamma_{kj}(\boldsymbol{\xi}) = \delta_{ij}$; $F_{ij} = -\Gamma^{-1}_{ik}(\boldsymbol{\lambda})\tilde{C}_{klms}\Gamma^{-1}_{mj}(\boldsymbol{\lambda})(\tau_l\lambda_s + \tau_s\lambda_l)$; $\mu_{kpq} = \tau_k\lambda_p\lambda_q + \lambda_k\tau_p\lambda_q + \lambda_k\lambda_p\tau_q$; CPV stands for the Cauchy Principal Value of the integral ,and HFP stands for the Hadamard Finite Part of the integral.

In the solution of the boundary integral equations (3), (4) the sought functions are tractions t_i or displacements u_i on the boundary $\partial\mathcal{B}$ of the solid, and displacement discontinuity Δu_i on the crack surface C. When all of these functions are known, stress at arbitrary internal point $\mathbf{y} \in \mathcal{B}$ can be determined as

$$\begin{aligned}\sigma_{ij}(\mathbf{y}) = &\iint_{\partial\mathcal{B}}\left(D_{ijk}(\mathbf{x},\mathbf{y})t_k(\mathbf{x}) - S_{ijk}(\mathbf{x},\mathbf{y})u_k(\mathbf{x})\right)dS(\mathbf{x})\\ &+\iint_{C}\left(D_{ijk}(\mathbf{x},\mathbf{y})\Sigma t_k(\mathbf{x}) - S_{ijk}(\mathbf{x},\mathbf{y})\Delta u_k(\mathbf{x})\right)dS(\mathbf{x})\\ &+\iiint_{\mathcal{B}} D_{ijk}(\mathbf{x},\mathbf{y})\, f_k(\mathbf{x})\,dV(\mathbf{x}).\end{aligned} \tag{8}$$

It should be mentioned that stress field possess square root singularity near crack front. The same as in 2D fracture mechanics stress intensity factors are introduced for 3D problems, which describe the strength of this square root singularity and serves as main fracture parameters. Thus accurate determination of the stress intensity factors is a very important issue.

3. Boundary element solution of the integral equations

3.1. Evaluation of anisotropic kernels

When implemented in BEM analysis for 3D cases, kernels given in the integral form can require tremendous computational efforts, which perhaps can involve millions of computations for a simple 3D model. Therefore, it is essential to use special techniques for evaluation of kernels. For instance, for the kernel (5) and its derivatives (7) (required for obtaining kernels (5), (6)) Xie et al. [14, p. 38] proposed three techniques, one of which is based on the direct numerical integration, and two others incorporate the residue theorem and reduce kernel evaluation to the Stroh eigenvalue problem.

The computational complexity of the direct numerical integration is $m \cdot O(n^3)$, where m is a number of quadrature nodes, and n is the dimension of the problem (3 for anisotropic materials), since matrix inversion is incorporated in kernels evaluation. The computational complexity of the Stroh eigenvalue problem is $\frac{2}{3}(2n)^3 + O(n^2) \approx 5.3n^3 + O(n^2)$ (if Householder transformations are used) or even higher. Therefore, computational costs of direct numerical integration are comparable to those of residue calculus, if the number of nodes is approximately about 10. However, special case of repeated eigenvalues should be considered separately in the residue calculus approach, which complicates corresponding computational algorithms. Thus, direct numerical integration approach is advantageous; however, one has to find the numerical quadrature, which provides the best accuracy at small number of nodes.

Since

$$\boldsymbol{\lambda} = \mathbf{n}\cos\phi + \mathbf{m}\sin\phi, \tag{9}$$

where $\mathbf{n}$ and $\mathbf{m}$ are two arbitrary orthogonal vectors in the oblique plane normal to $\mathbf{t}$, it is easy to show that the integrands in (5)–(7) are π-periodic functions in polar angle ϕ. Xie et al. [15, p. 183] used Gaussian quadrature for evaluation of these integrals. However, even at 25 Gaussian points the convergence of the results, especially for the second derivative, is not satisfactory.

Therefore, in this study it is proposed to use the trapezoid formula for numerical integration of the integrals involved in kernels. At first glance, it seems unreasonable, since it is known that Gaussian quadrature has the highest accuracy for polynomials. However, it was recently shown that trapezoid rule is exponentially convergent for integrals over a periodic interval. This useful feature is implemented in calculation of kernels (5), (6).

In the numerical examples section it is shown high convergence of the trapezoid rule applied to calculation of the kernels.

3.2. Boundary element mesh and crack front modeling

At the first step (preprocessing) of the boundary element solution of derived boundary integral equations for a particular problem the surface $\partial\mathcal{B}$ of the solid along with the crack surface C is meshed with quadrilateral quadratic discontinuous boundary elements. The local curvilinear coordinate system $O\xi\eta$ is associated with each boundary element, moreover, $-1 \le \xi \le 1$, $-1 \le \eta \le 1$. The collocation points are placed at nodes $\xi = (-2/3; 0; 2/3)$; $\eta = (-2/3; 0; 2/3)$. Therefore, there are 9 collocation points associated with each boundary element.

Boundary conditions along with unknown boundary and discontinuity functions are interpolated within the collocation points at each boundary element Γ_N as

$$\mathbf{b}_N(\xi,\eta)=\sum_{i=1}^{3}\sum_{j=1}^{3}\mathbf{b}_N^{i,j}\phi_i(\xi)\phi_j(\eta), \tag{10}$$

where $\mathbf{b}=\left(u_i,\Delta u_i,t_i,\Sigma t_i,\Delta t_i\right)^{\mathrm{T}}$, and the discontinuous shape functions are given as [2]

$$\phi_1(\xi)=\xi\left(\frac{9}{8}\xi-\frac{3}{4}\right),\quad \phi_2(\xi)=\left(1-\frac{3}{2}\xi\right)\left(1+\frac{3}{2}\xi\right),\quad \phi_3(\xi)=\xi\left(\frac{9}{8}\xi+\frac{3}{4}\right). \tag{11}$$

If the side of the boundary element models the crack front, special shape functions are used for displacement and temperature discontinuity to capture the square root singularity arising at crack front

$$\phi_i^{\Lambda}(\xi)=\sqrt{1\pm\xi}\left(\Phi_{i1}^{\Lambda}+\sum_{j=2}^{3}\Phi_{ij}^{\Lambda}(1\pm\xi)^{j-1}\right). \tag{12}$$

Constants Φ_{ij}^{Λ} are determined from the system of equations $\phi_i\left(\xi_j\right)=\delta_{ij}$, where $\xi_j=\left(-2/3;0;2/3\right)$.

Substituting (10) into the boundary integral equations (3), (4), one obtains the system of linear algebraic equations for unknown nodal values of the boundary and discontinuity functions.

3.3. Techniques for precise integration of regular, weakly, strongly and hypersingular integrals

The coefficients of the obtained system of algebraic equations are the double integrals

$$I_{NijIJ}^{(1)}(\mathbf{x}_0)=\int_{-1}^{1}\int_{-1}^{1}U_{IJ}\left(\mathbf{x}(\xi,\eta),\mathbf{x}_0\right)\phi_i(\xi)\phi_j(\eta)J_N(\xi,\eta)d\xi d\eta,$$

$$I_{NijIJ}^{(2)}(\mathbf{x}_0)=\int_{-1}^{1}\int_{-1}^{1}T_{IJ}\left(\mathbf{x}(\xi,\eta),\mathbf{x}_0\right)\phi_i(\xi)\phi_j(\eta)J_N(\xi,\eta)d\xi d\eta,$$

$$I_{NijIkJ}^{(3)}(\mathbf{x}_0)=\int_{-1}^{1}\int_{-1}^{1}D_{IkJ}\left(\mathbf{x}(\xi,\eta),\mathbf{x}_0\right)\phi_i(\xi)\phi_j(\eta)J_N(\xi,\eta)d\xi d\eta,$$

$$I_{NijIkJ}^{(4)}(\mathbf{x}_0)=\int_{-1}^{1}\int_{-1}^{1}S_{IkJ}\left(\mathbf{x}(\xi,\eta),\mathbf{x}_0\right)\phi_i(\xi)\phi_j(\eta)J_N(\xi,\eta)d\xi d\eta,$$

where $J_N(\xi,\eta)=\left|\frac{\partial\mathbf{x}}{\partial\xi}\times\frac{\partial\mathbf{x}}{\partial\eta}\right|$ is a Jacobian of variable change on the boundary element Γ_N.

Since the shape functions $\phi_i(\xi)$, $\phi_j(\eta)$ can be selected in the form (12) for elements, which model the crack front, customary Gaussian quadrature can produce high error, even if the collocation point $\mathbf{x}_0$ does not belong to the boundary element Γ_N. Therefore, in the present boundary element formulation the following polynomial mapping is used

$$\xi=\frac{1}{2}\left(3-\xi_1^2\right)\xi_1,\quad \eta=\frac{1}{2}\left(3-\eta_1^2\right)\eta_1,\quad d\xi d\eta=\frac{9}{4}\left(1-\xi_1^2\right)\left(1-\eta_1^2\right)d\xi_1 d\eta_1, \tag{13}$$

which maps the domain $(-1;1)\times(-1;1)$ onto itself and smoothens the integrand at $\xi_1=\pm1$; $\eta_1=\pm1$. After (13) is applied, the regular integrals are evaluated numerically with Gaussian quadrature (20 nodes are used).

Special attention should be paid to the case, when $\mathbf{x}_0=\mathbf{x}\left(\xi^0,\eta^0\right)$ belongs to the boundary element Γ_N. From Eqs (3) – (7) it follows that in this case integral $I^{(1)}$ is weakly singular, $I^{(2)}$, $I^{(3)}$ are strongly singular, and $I^{(4)}$ is hypersingular. All these integrals are evaluated in the polar coordinate system, which yield

$$I=\frac{9}{4}\sum_{q=1}^{4}\int_{\theta_q}^{\theta_{q+1}}\int_{0}^{R_q(\theta)}F\left(\mathbf{x}(\xi,\eta),\mathbf{x}_0\right)\phi_i(\xi)\phi_j(\eta)J_N(\xi,\eta)\left(1-\xi_1^2\right)\left(1-\eta_1^2\right)r\,dr\,d\theta, \tag{14}$$

where $F\left(\mathbf{x}(\xi,\eta)-\mathbf{x}_0\right)$ is a corresponding kernel; $\xi=\xi\left(\xi_1^0+r\cos\theta\right)$, $\eta=\eta\left(\eta_1^0+r\sin\theta\right)$; $\mathbf{x}_0=\mathbf{x}\left(\xi^0,\eta^0\right)$ ($\xi^0=\xi\left(\xi_1^0\right)$, $\eta^0=\eta\left(\eta_1^0\right)$) is a collocation point at the boundary element Γ_N; $\theta_1=\arctan\left(-1-\eta_1^0,1-\xi_1^0\right)$, $\theta_2=\arctan\left(1-\eta_1^0,1-\xi_1^0\right)$, $\theta_3=\arctan\left(1-\eta_1^0,-1-\xi_1^0\right)$; $\theta_4=2\pi+\arctan\left(-1-\eta_1^0,-1-\xi_0\right)$; $\theta_5=2\pi+\theta_1$; $R_1(\theta)=\left(1-\xi_1^0\right)/\cos\theta$; $R_2(\theta)=\left(1-\eta_1^0\right)/\sin\theta$; $R_3(\theta)=\left(-1-\xi_1^0\right)/\cos\theta$; $R_4(\theta)=\left(-1-\eta_1^0\right)/\sin\theta$.

It is readily seen from Eq (14) that if the kernel $F\left(\mathbf{x},\mathbf{x}_0\right)$ is weakly singular $\left(F\sim1/r\right)$ integral (14) is regular, since the polar transformation Jacobian cancels this singularity. Therefore, convenient Gaussian quadrature rule can be applied to evaluate this integral numerically.

For numerical evaluation of singular ($F \sim 1/r^2$) and hypersingular ($F \sim 1/r^3$) integrals Pan and Yuan [10, p. 211] proposed to use the finite part Kutt's numerical quadrature [18, p. 40] for inner integral with respect to r and Gaussian quadrature for the outer regular integral with respect to θ.

However, the main problem of the Kutt's quadrature used by Pan and Yuan [10, p. 211] is the requirement of evaluation of the singularity coefficient at the point $\mathbf{x}_0$, which depend on the vector $\mathbf{x}-\mathbf{x}_0$. The latter is influenced by the geometry of the boundary element. Pan and Yuan [10, p. 211] considered only planar elements. When non-planar boundary elements are considered, analytic determination of the dependence of kernel singularity coefficient on boundary element curvilinear coordinates ξ, η produce formulae, which are hard to implement in the computer code. Therefore, here Kutt's quadrature is modified to omit the requirement of computation of singularity coefficient and to be more accurate.

Kutt [19, p. 205] proposed the following quadrature rule for finite part integrals with algebraic singularity

$$\mathrm{HFP}\int_0^R \frac{f(x)}{x^\lambda}dx \approx R^{1-\lambda}\sum_{i=1}^{N}\left[w_i^{(\lambda)}+c_i^{(\lambda)}\frac{\ln R}{(\lambda-1)!}\right]f(Rt_i), \tag{15}$$

where $t_i \in [0;1]$ are quadrature nodes; λ is a positive integer, which indicates the strength of singularity; $R>0$; $w_i^{(\lambda)}$ and $c_i^{(\lambda)}$ are weights for the selected λ and t_i $(i=1,...,N)$. The latter are determined from the following system of linear algebraic equations

$$\sum_{j=1}^{N} w_j^{(\lambda)} t_j^{(i-1)} = \begin{cases} \dfrac{1}{i-\lambda}, & i\neq\lambda, \\ 0, \quad \text{otherwise}; \end{cases}, \quad \sum_{j=1}^{N} c_j^{(\lambda)} t_j^{(i-1)} = \begin{cases} (\lambda-1)!, & i=\lambda, \\ 0, \quad \text{otherwise}; \end{cases} \quad (i=1,...,N). \tag{16}$$

Due to its polynomial interpolation nature, Kutt's quadrature is exact for polynomials of degree $N-1$.

Kutt has selected the equidistant node set $t_i=(i-1)/N$ [18, p. 40]. The same nodes were used by Pan and Yuan [10, p. 211] for numerical evaluation of hypersingular integrals in their 3D BEM. However, this set of quadrature nodes has two inconveniencies, when implemented in BEM. The first one is that one has to know $f(0)$. Since in the BEM it is not given explicitly, one should consider the integrand behavior at a singular point separately, which is difficult in the case of non-planar geometries. The second is that for high numbers N of quadrature nodes Runge's phenomenon can be observed, which can lead to sufficient errors, when integrating certain functions. These inconveniences can be overcome if one select Chebyshev nodes as the nodes of Kutt's quadrature

$$t_i = \frac{1}{2}\left(1-\cos\frac{(2i-1)\pi}{2N}\right) \quad (i=1,...,N). \tag{17}$$

Numerical tests on polynomials of degree higher than $N-1$ have shown that the error of the modified Kutt's quadrature with Chebyshev nodes is much less than those of the convenient Kutt's quadrature with equidistant nodes.

With respect to this, inner finite part integrals are evaluated via Eq (15) assuming that

$$f(r) = F(\mathbf{x}(\xi,\eta),\mathbf{x}_0)\phi_i(\xi)\phi_j(\xi)J_N(\xi,\eta)(1-\xi_1^2)(1-\eta_1^2)r^{\lambda+1}, \tag{18}$$

where $\lambda+1$ is the strength of singularity of the kernel $F(\mathbf{x},\mathbf{x}_0)$. Since Chebyshev nodes (17) used in the quadrature (15) do not require to evaluate $f(0)$, no other special treatment of singular terms is required, which is advantageous comparing to the usage of convenient Kutt's quadrature utilized by Pan and Yuan [10, p. 211].

3.4. Stress intensity factors at crack front

Consider a local coordinate system at a point A of the crack front (Figure 1). The axes of this system are defined by three unit orthogonal vectors $\mathbf{n}$, $\mathbf{m}$, $\boldsymbol{\tau}$, where $\mathbf{n}$ is a normal to crack face; $\mathbf{m}$ is a tangent to the crack front curve at A, and $\boldsymbol{\tau}=\mathbf{n}\times\mathbf{m}$. Without loss in generality consider that the boundary element, which the point A belongs to, models the crack front line with its side $\xi=1$ (Figure 1).

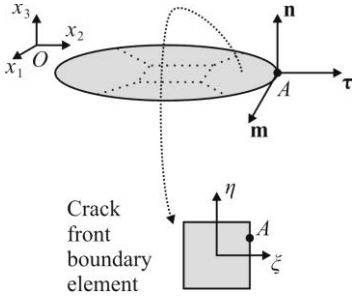

Figure 1. Local coordinate system at crack front

Normal and tangent vectors are defined as

$$\mathbf{n}=\left(\frac{\partial\mathbf{x}}{\partial\xi}\times\frac{\partial\mathbf{x}}{\partial\eta}\right)\Bigg/\left|\frac{\partial\mathbf{x}}{\partial\xi}\times\frac{\partial\mathbf{x}}{\partial\eta}\right|;\quad \mathbf{m}=-\frac{\partial\mathbf{x}}{\partial\eta}\Bigg/\left|\frac{\partial\mathbf{x}}{\partial\eta}\right|, \tag{19}$$

where $\mathbf{x}(\xi,\eta)$ is a position vector, which defines the surface of the boundary element. Then according to Eq (10) the displacement discontinuity function $\Delta\mathbf{u}^{*}(\mathbf{x})$ in the local coordinate system on the considered boundary element is equal to

$$\Delta\mathbf{u}^{*}(\mathbf{x})=\mathbf{\Omega}\sum_{i=1}^{3}\sum_{j=1}^{3}\Delta\mathbf{u}^{(i,j)}\phi_i^{\Delta}(\xi)\phi_j(\eta), \tag{20}$$

where $\Delta\mathbf{u}^{(i,j)}$ are the nodal values of the displacement discontinuity function, and $\mathbf{\Omega}$ is the rotation matrix, which is defined as

$$\mathbf{\Omega}=\begin{bmatrix}\tau_1 & n_1 & m_1\\ \tau_2 & n_2 & m_2\\ \tau_3 & n_3 & m_3\end{bmatrix}. \tag{21}$$

According to the stress intensity factors vector at the point A of the crack front is defined as

$$\mathbf{k}=\lim_{\mathbf{x}\to\mathbf{x}(A)}\sqrt{\frac{\pi}{8s(\mathbf{x})}}\mathbf{L}\cdot\Delta\tilde{\mathbf{u}}^{*}(\mathbf{x}), \tag{22}$$

where $\mathbf{k}=\left[K_{\mathrm{II}},K_{\mathrm{I}},K_{\mathrm{III}}\right]^{\mathrm{T}}$; K_{I}, K_{II}, K_{III} are the stress intensity factors of corresponding modes; $\mathbf{L}$ is a Barnett – Lothe tensor evaluated in the local coordinate system; and $s(\mathbf{x})$ is an arc length evaluated from $\mathbf{x}$ to A along the cross section of the crack with the plane $(\mathbf{n},\boldsymbol{\tau})$.

Expanding $s(\mathbf{x})$ into Taylor series at the vicinity of A one obtains

$$s=(1-\xi)\rho(\eta_A)+O\left((1-\xi)^2;(\eta_A-\eta)^2\right), \tag{23}$$

where

$$\rho(\eta_A)=\boldsymbol{\tau}\cdot\left.\frac{\partial\mathbf{x}}{\partial\xi}\right|_{\xi=1,\eta=\eta_A}. \tag{24}$$

Substituting (12) and (23) into (22) and evaluating the limit one obtains

$$\mathbf{k}=\sqrt{\frac{\pi}{8\rho(\eta_A)}}\mathbf{L}\cdot\mathbf{\Omega}\sum_{i=1}^{3}\sum_{j=1}^{3}\Delta\mathbf{u}^{(i,j)}\Phi_{i1}^{\Delta}\phi_j(\eta_A), \tag{25}$$

which is the formula implemented in the present BEM for precise evaluation of the stress intensity factors.

According to [11, p. 96] the Barnett – Lothe tensor in the local coordinate system can be evaluated with the following integral

$$\mathbf{L}=-\frac{1}{\pi}\int_0^{\pi}\mathbf{\Omega}\mathbf{N}_3(\theta)\mathbf{\Omega}^{\mathrm{T}}d\theta, \tag{26}$$

where $\mathbf{N}_3(\theta)=-\mathbf{R}(\theta)\mathbf{T}^{-1}(\theta)\mathbf{R}^{\mathrm{T}}(\theta)-\mathbf{Q}(\theta)$; $Q_{ij}(\theta)=C_{ikjm}\omega_k\omega_m$, $T_{ij}(\theta)=C_{ikjm}\vartheta_k\vartheta_m$, $R_{ij}(\theta)=C_{ikjm}\omega_k\vartheta_m$; $\boldsymbol{\omega}=\boldsymbol{\tau}\cos\theta+\mathbf{n}\sin\theta$, $\boldsymbol{\vartheta}=-\boldsymbol{\tau}\sin\theta+\mathbf{n}\cos\theta$.

4. Numerical results

4.1. Fast convergence of the trapezoid rule in evaluation of anisotropic kernels

Since at first glance it is not obvious that the trapezoid rule can efficiently handle evaluation of anisotropic kernels, we consider an example of Xie et al. [14] of numerical evaluation of the second derivative $U_{IJ,km}$ of elastic Green's function. The results are obtained for Mg material with the following elastic properties [14]: $C_{11}=C_{22}=59.7$ GPa, $C_{33}=61.7$ GPa, $C_{13}=C_{23}=21.7$ GPa, $C_{12}=26.2$ GPa, $C_{44}=C_{55}=16.4$ GPa, $C_{66}=16.75$ GPa.

Second derivative of the Green's function is evaluated at the point $\mathbf{x}-\mathbf{x}_0=(1,2,3)^{\mathrm{T}}$. Four methods are compared. They are the Numerical Integration Method (NIM) [14], the Residue Calculus Method (RCM) [14, p. 38], the improved Residue Calculus Method (iRCM) [14, p. 38], and the proposed numerical integration with the Trapezoid Rule (TR). Since the worst convergence is possessed by $U_{22,11}$ [14, p. 38], only its value is presented in Table 1. The exact solution is taken from Pan and Chou [20, p. 10]. Numerical calculations are held

with the developed C++ program, which uses IEEE 64-bit double precision floating point number format (with 15–17 significant decimal digits).

It can be seen from Table 1 that the trapezoid rule converges very fast. Only 16 nodes of the trapezoid rule are enough to obtain the same accuracy as the Gaussian quadrature with 25 nodes or the improved RCM. The 8-point trapezoid rule has the accuracy comparable with the RCM.

Comparison of the results for different number of the trapezoid rule nodes allows to state that the number of true significant decimal digits is proportional to the number of nodal points in the trapezoid rule. However, the number of true decimal digits is also limited with the length of the mantissa used in floating-point computations.

Table 1

$U_{22,11}$ evaluated by different approaches at the given point of Mg anisotropic medium

Exact	$-$**6.2581146860784102** $\times 10^{-5}$	$\times 10^{9}$ m^{-1}/N
NIM with 25 Gaussian points	$-$**6.258114686078**3276 $\times 10^{-5}$	
RCM	$-$**6.25811**47470664643 $\times 10^{-5}$	
iRCM	$-$**6.258114686078**3736 $\times 10^{-5}$	
TR with 4 points	$-$**6.2**67696062871067 $\times 10^{-5}$	
TR with 8 points	$-$**6.25811**2576749089 $\times 10^{-5}$	
TR with 12 points	$-$**6.258114686**298868 $\times 10^{-5}$	
TR with 16 points	$-$**6.258114686078**395 $\times 10^{-5}$	
TR with 20 points	$-$**6.258114686078**408 $\times 10^{-5}$	

4.2. Numerical verification. Penny-shaped crack in an infinite isotropic medium

In order to verify the developed BEM consider the thermoelastic problem for a penny-shaped crack of radius R, which is parallel to Ox_1x_2 plane. The crack is meshed with only 12 quadrilateral discontinuous boundary elements (Figure 2). Four central boundary elements Nos. 1–4 use general quadratic shape functions (11), while other elements (Nos. 5–12) utilize special shape functions (12) to account for the square root singularity of stress at the crack front. Thus the reduced numerical problem has 12x9x3=324 degrees of freedom.

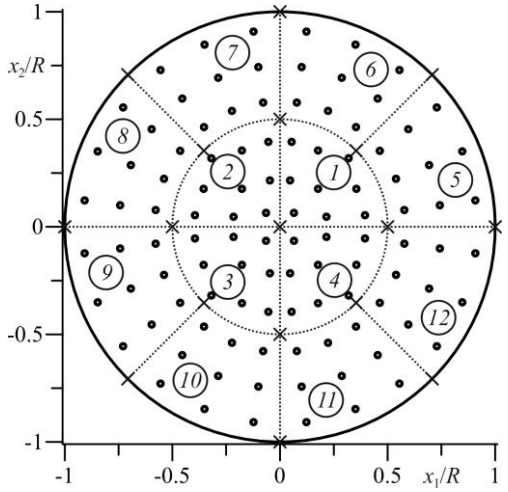

Figure 2. Boundary element mesh of the penny-shaped crack

The medium is loaded with uniform stress field $\sigma_{33} = p$ at infinity. According to [21, p. 15], in this case the analytic solution of the problem gives the following value of stress intensity factor $K_{\mathrm{I}}^{0} = p\sqrt{R/\pi}$. Normalized values of the stress intensity factor K_{I} along the crack front line defined by polar angle φ are depicted in Figure 3.

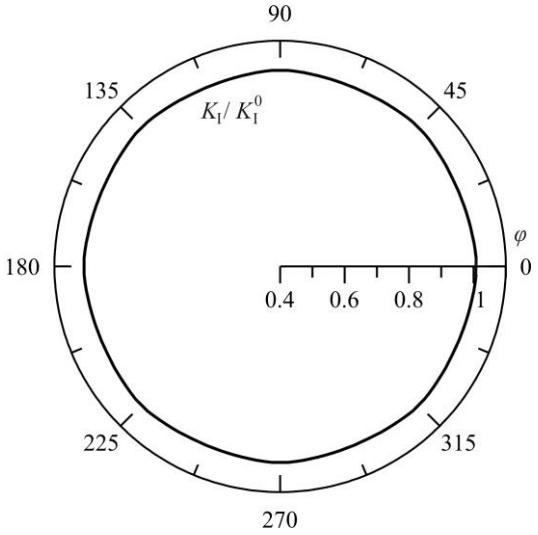

Figure 3. Numerically obtained stress intensity factor along a front line of the penny-shaped crack

Figure 1 shows that the stress intensity factor K_I is constant along crack front. Detailed analysis of numerical data has shown that relative error of computations is less than 0.9 %. Thus present boundary element approach allows precise study of stress intensity factors with low number of elements.

4.3. Paraboloidal crack in anisotropic medium

Consider anisotropic Mg medium (which properties are given in section 4.1) containing a crack, which surface is given by the following equation of elliptic paraboloid of revolution

$$x_3 = \rho\left(x_1^2 + x_2^2\right), \quad x_1^2 + x_2^2 \le R^2, \tag{27}$$

where ρ and R are constants (if $\rho = 0$ one obtains a penny-shaped crack of a radius R). The crack is meshed with only 12 quadrilateral discontinuous boundary elements, which x_1 and x_2 coordinates are the same as depicted in Figure 2, and x_3 coordinate is determined through Eq (27). The medium is loaded with uniform stress field $\sigma_{33} = p$ at infinity. Normalized values of stress intensity factors at crack front are depicted in Figure 4. The normalization factor is equal to $K_0 = K_I^0 = p\sqrt{R/\pi}$.

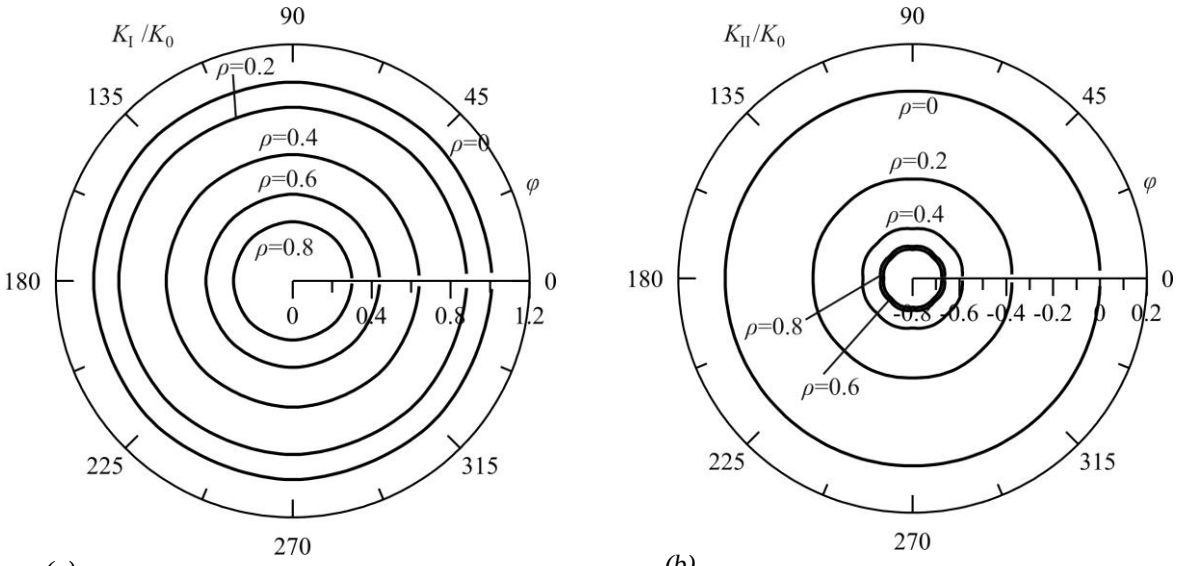

Figure 4. Normalized stress intensity factors along a front line of paraboloidal crack: (a) normal mode SIF K_I; (b) shearing mode SIF K_{II}.

Figure 4 shows that SIF K_{I} decrease with increase in ρ, while K_{II} increase in magnitude. This is obvious, since non-planar crack exhibits shearing mode opening due to its geometry and direction of the applied loading. Since crack front line is parallel to isotropy plane of the materials, both stress intensity factors are constant along the front line. Also it should be noted that material anisotropy in the case of a penny-shaped crack ($\rho = 0$) does not affect stress intensity factor; it is the same as for isotropic case.

4. Discussion

The paper presents fast and accurate boundary element method for fracture mechanics analysis of anisotropic solids with 3D cracks. Several novelties are introduced, which allow derivation of the efficient boundary element approach. The first of them is application of the trapezoid rule to evaluation of anisotropic kernels. Due to its simplicity and exponential convergence for integrals over a periodic interval it allows accurate and fast evaluation of the kernels, which is essentially important in the derivation of fast BEM. The second is the usage of polynomial mappings and modified Kutt's quadratures for finite part integrals, which allows accurate numerical integration of singular and hypersingular integrals without additional treatment of singular terms, which is advantageous for non-planar geometries. The third is an introduction of special shape functions for the displacement discontinuity at the crack, which allows accurate determination of the field intensity factors.

These novelties allowed derivation of the efficient 3D BEM, which allows studying both isotropic and anisotropic linear elastic materials with cracks of arbitrary shape. The numerical examples presented prove high accuracy of the present boundary element formulation.

Present approach can be combined with Sih's strain energy density criterion to study 3D cracks propagation in anisotropic elastic solids under fatigue loading, which is the direction of future research.

References:

1. Sih, G.C. (1991), *Mechanics of fracture initiation and propagation*, Kluwer Academic Publishers, The Netherlands.
2. Mi, Y. and Aliabadi, M.H. (1992), «Dual boundary element method for three-dimensional fracture mechanics analysis», *Engineering Analysis with Boundary Elements*, No. 10, pp. 161–171.
3. Guiggiani, M., Krishnasamy, G., Rizzo, F.J. and Rudolphi, T.J. (1991), «Hypersingular boundary integral equations: A new approach to their numerical treatment», *Boundary Integral Methods, Theory and Applications*, Springer-Verlag, Berlin, pp. 211–220.
4. Lv, J.-H., Feng, X.-T., Yan, F. and Chen, B.-R. (2016), «Implementation of CPCT based BIEs for 3D elasticity and its application in fracture mechanics», *Engineering Analysis with Boundary Elements*, No. 71, pp. 1–10.
5. Saez, A., Ariza, M.P. and Dominguez, J. (1997), «Three-dimensional fracture analysis in transversely isotropic solids», *Engineering Analysis with Boundary Elements*, No. 20, pp. 287–298.
6. Muñoz-Reja, M.M., Buroni, F.C., Sáez, A. and García-Sánchez, F. (2016), «3D explicit-BEM fracture analysis for materials with anisotropic multifield coupling», *Applied Mathematical Modelling*, No. 40, pp. 2897–2912.
7. Jaworski, D., Linkov, A. and Rybarska-Rusinek, L. (2016), «On solving 3D elasticity problems for inhomogeneous region with cracks, pores and inclusions», *Computers and Geotechnics*, No. 71, pp. 295–309.
8. Nikolskiy, D.V., Mogilevskaya, S.G. and Labuz, J.F. (2015), «Boundary element analysis of non-planar three-dimensional cracks using complex variables», *International Journal of Rock Mechanics & Mining Sciences*, No. 76, pp. 44–54.
9. Aimi, A. and Diligenti, M. (2002), «Hypersingular kernel integration in 3D Galerkin boundary element method», *Journal of Computational and Applied Mathematics*, No. 138, pp. 51–72.
10. Pan, E. and Yuan, F.G. (2000), «Boundary element analysis of three-dimensional cracks in anisotropic solids», *Int. J. Numer. Meth. Engng.*, No. 48, pp. 211–237.
11. Ting, T.C.T. (1996), *Anisotropic elasticity: theory and applications*, Oxford University Press, Oxford.
12. Buroni, F.C. and Sáez, A. (2010), «Three-dimensional Green's function and its derivative for materials with general anisotropic magneto-electro-elastic coupling». *Proc R Soc A*, No. 466, pp. 515–537.
13. Barber, J.R. (2010), *Elasticity*, Springer, London.
14. Xie, L., Zhang, C., Hwu, C., Sladek, J. and Sladek, V. (2016), «A comparison of three evaluation methods for Green's function and its derivatives for 3D generally anisotropic solids», *European Journal of Computational Mechanics*, [Online], available at: http://dx.doi.org/10.1080/17797179.2016.1181039
15. Xie, L., Zhang, C., Hwu, C., Sladek, J. and Sladek, V. (2015), «On two accurate methods for computing 3D Green's function and its first and second derivatives in piezoelectricity», *Engineering Analysis with Boundary Elements*, No. 61, pp. 183–193.
16. Weideman, J.A.C. (2002), «Numerical integration of periodic functions: a few examples», *The American Mathematical Monthly*, No. 109, pp. 21–36.
17. Trefethen, L.N. and Weideman, J.A.C. (2014), «The exponentially convergent trapezoidal rule», *SIAM Review*, No. 56, pp. 385–458.
18. Kutt, H.R. (1975), *On the numerical evaluation of finite-part integrals involving an algebraic singularity*, PhD thesis, University of Stellenbosch.
19. Kutt, H.R. (1975), «The numerical evaluation of principal value integrals by finite-part integration», *Numer. Math.*, No. 24, pp. 205–210.

20. Pan, Y.C. and Chou, T.W. (1976), «Point force solution for an infinite transversely isotropic solid», *Journal of Applied Mechanics*, No. 43, pp. 608–612.
21. Murakami, Y. (ed.) (1987), *Stress Intensity Factors Handbook*, In 2 Vol., Pergamon press, Oxford.

Ilchuk Nataliia – PhD, Associated Professor, Department of Construction and Civil Engineering, Lutsk National Technical University, Ukraine.

Scientific interests:
– Boundary element;
– paraboloidal crack;
– anisotropy;
– intensity factor;
– isotropic medium;
– solids.

E-mail: natali2507.ua@gmail.com.

Pasternak Iaroslav – PhD, DSc, Professor, Head of Department of Applied Mathematics and Mechanics, Lutsk National Technical University, Ukraine.

Scientific interests:
– Boundary element;
– mechanics analysis;
– anisotropic solids;
– non-planar cracks;
– intensity factors;
– isotropic medium.

E-mail: iaroslav.m.pasternak@gmail.com.

Article was received by the editorial staff 26.03.2019.